

Scalar Casimir Energies of Tetrahedra and Prisms

E. K. Abalo* and K. A. Milton†

*Homer L. Dodge Department of Physics and Astronomy,
University of Oklahoma, Norman, OK 73019*

L. Kaplan‡

Department of Physics, Tulane University, New Orleans, LA 70118

(Dated: April 20, 2022)

Abstract

New results for scalar Casimir self-energies arising from interior modes are presented for the three integrable tetrahedral cavities. Since the eigenmodes are all known, the energies can be directly evaluated by mode summation, with a point-splitting regulator, which amounts to evaluation of the cylinder kernel. The correct Weyl divergences, depending on the volume, surface area, and the edges, are obtained, which is strong evidence that the counting of modes is correct. Because there is no curvature, the finite part of the quantum energy may be unambiguously extracted. Cubic, rectangular parallelepipedal, triangular prismatic, and spherical geometries are also revisited. Dirichlet and Neumann boundary conditions are considered for all geometries. Systematic behavior of the energy in terms of geometric invariants for these different cavities is explored. Smooth interpolation between short and long prisms is further demonstrated. When scaled by the ratio of the volume to the surface area, the energies for the tetrahedra and the prisms of maximal isoareal quotient lie very close to a universal curve. The physical significance of these results is discussed.

PACS numbers: 03.70.+k, 11.10.Gh, 42.50.Lc, 42.50.Pq

*Electronic address: abalo@nhn.ou.edu

†Electronic address: milton@nhn.ou.edu

‡Electronic address: lkaplan@tulane.edu

I. INTRODUCTION

The concept of Casimir self-energy remains elusive. Since 1948, the year of H. B. G. Casimir's seminal paper [1], what is now called the Casimir effect has captivated many. Casimir discovered an attractive quantum vacuum force between uncharged parallel conducting plates. Yet, while Casimir later extrapolated from this to predict an attractive force for a spherical conducting shell [2], Boyer proved the self-stress in that case to be instead repulsive, which was an even more unexpected result [3]. Since Boyer's formidable calculation, many other configurations were examined: cylinders, boxes, wedges, etc. The literature abounds with these results; for a review see Ref. [4]. However, since there are other well-known cases of cavities where the interior modes are known exactly, it is surprising that essentially no attention had been paid to these. For example, recently we presented the first results for Casimir self-energies for cylinders of equilateral, hemiequilateral, and right isosceles triangular cross sections [5], even though the spectrum is well-known and appears in general textbooks [6, 7]. Possibly, the reason for this neglect was that only interior modes could be included for any of these cases, unlike the case of a circular cylinder, where both interior and exterior modes must be included in order to obtain a finite self-energy. However, the extensive attention to rectangular cavities puts the lie to this hypothesis [8–13]. It seems not to have been generally appreciated that finite results can be obtained in all these cases because there are no curvature divergences for boxes constructed from plane surfaces.

In this paper, as in Ref. [5], we put aside the serious objection that these self-energies may be impossible to observe, even in principle.¹ For example, the positive self-energy of a spherical shell is not the negative of the work required to separate two hemispheres, which must be positive. We also are unable to comment on the exterior contributions to the Casimir energy, which would be extremely difficult to calculate for any of these boxes, since the Helmholtz equation is not separable exterior to any box with flat sides. Nonetheless, except for geometries with smooth boundaries, one would expect an interesting progression solely for interior energies. The fact that a smooth uniform behavior is observed suggests that a physical/mathematical significance lies here. Also the interior Casimir energy can

¹ The exception would be in the coupling to gravity. Since it is highly likely that Casimir energies obey the equivalence principle [14], we expect that like any other contribution to the self-energy of a body, the Casimir energy would contribute to the inertial and gravitational mass of a body [15, 16].

be relevant to physical situations; for example, the interior zero-point energy of gluons is of crucial significance for the bag model of hadrons, where the fields exist only inside the cavity [17].

In Ref. [5] we obtained exact, closed-form results for the three above-mentioned integrable triangles, both in a plane, and for cylinders with the corresponding cross section, for Dirichlet, Neumann, and perfect conducting boundary conditions. The expected Weyl divergences related to the area, perimeter, and the corners of the triangles were obtained, going a long way toward verifying the counting of modes, which is the most difficult aspect of these calculations. Moreover, we were able to successfully interpolate between the results for these triangles by using an efficient numerical evaluation, and showed that the energies lie on a smooth curve, which was reasonably well-approximated by the result of a proximity force calculation. In this paper we show that the same techniques can be applied to tetrahedral boxes; again, there are exactly three integrable cases, where an explicit spectrum can be written down. Again, it is surprising that the Casimir energies for these cases are not well-known. The only treatment of a pyramidal box found in the Casimir energy literature appears in a relatively unknown work of Ahmedov and Duru [18], which, however, seems to contain a counting error.

In this paper we present Casimir energy calculations for the three integrable tetrahedra. For each cavity we consider a massless scalar field subject to Dirichlet and Neumann boundary conditions on the surfaces. We regulate the mode summation by temporal point-splitting, which amounts to evaluation of what is called the cylinder kernel [19], and extract both divergent (as the regulator goes to zero) and finite contributions to the energy. We also revisit cubic, rectangular parallelepipedal, triangular prismatic, and spherical geometries with the same boundary conditions. In the end, we explore the functional behavior of the Casimir energies with respect to an appropriately chosen ratio of the cavities' volumes and surface areas. We also examine limits as the prism length tends to zero and infinity, which correspond to the Casimir parallel plate and infinite cylinder limits, respectively.

A. Point-splitting regularization

We regularize our results by temporal point-splitting. As explained in Ref. [5], after a Euclidean rotation, we obtain

$$E = \frac{1}{2} \lim_{\tau \rightarrow 0} \left(-\frac{d}{d\tau} \right) \sum_{kmn} e^{-\tau \sqrt{\lambda_{kmn}^2}}, \quad (1.1)$$

where the sum is over the quantum numbers that characterize the eigenvalues, and τ is the Euclidean time-splitting parameter, supposed to tend to zero at the end of the calculation. One recognizes the sum as the traced cylinder kernel [19]. Next, we proceed to re-express the sum with Poisson's summation formula.

B. Poisson resummation

Poisson's summation formula allows one to recast a slowly convergent sum into a more rapidly convergent sum of its Fourier transform,

$$\sum_{m=-\infty}^{\infty} f(m) = \sum_{n=-\infty}^{\infty} \left(\int_{-\infty}^{\infty} e^{2\pi i m n} f(m) dm \right). \quad (1.2)$$

By point-splitting and resumming, we are able to isolate the finite parts, which are Casimir self-energies, and the corresponding divergent parts, which are the Weyl terms (see Appendix A for more detail).

II. CASIMIR ENERGIES OF TETRAHEDRA

The three integrable tetrahedra mentioned above are not recent discoveries. They have, in fact, been the subject of a few articles [20–22]. However, there appears to be only one Casimir energy article concerning one of these tetrahedra, which we denote as the “small” tetrahedron [18]. These tetrahedra are integrable in the sense that their eigenvalue spectra are known explicitly, and there are no other such tetrahedra. We will successively look at the “large,” “medium,” and “small” tetrahedra, as defined below, and obtain interior scalar Casimir energies for Dirichlet and Neumann boundary conditions. Although the exterior problems cannot be solved in these cases, the finite parts of the interior energies are well defined because the curvature is zero, and hence the second heat kernel coefficient vanishes.

A. Large Tetrahedron

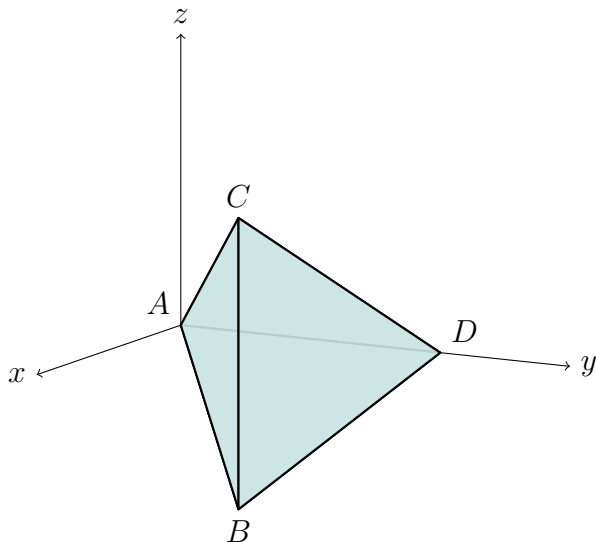


FIG. 1: Large tetrahedron: $-x < z < x$ and $x < y < 2a - x$.

The first tetrahedron, sketched in Fig. 1, which we denote “large,” is comparatively the largest or rather the most symmetrical. One can obtain a medium tetrahedron by bisecting a large tetrahedron and idem for the small and medium tetrahedra. One should note that the terms “large,” “medium,” and “small” are merely labels, since one can always rescale each tetrahedron independently of the others. The spectrum and complete eigenfunction set for the large tetrahedron, as well as those of the other tetrahedra, are known and appear in Ref. [20],

$$\lambda_{kmn}^2 = \frac{\pi^2}{4a^2} [3(k^2 + m^2 + n^2) - 2(km + kn + mn)] . \quad (2.1)$$

With Dirichlet and Neumann boundary conditions, different constraints are imposed on the spectrum, that is, on the ranges of the integers k , m , and n .

1. Dirichlet BC

The complete set of modes for Dirichlet boundary conditions is given by the restrictions $0 < k < m < n$. After extending the sums to all of (k, m, n) -space, we remove all the unphysical cases which are $k = 0$, $m = 0$, $n = 0$, $k = m$, $k = n$, and $m = n$ while keeping

track of the 24 degeneracies and compensating for oversubtractions. Finally, after suitable redefinitions of some individual terms, the Dirichlet Casimir energy for the large tetrahedron can be defined in terms of the function

$$g(p, q, r) = e^{-\tau\sqrt{(\pi/a)^2(p^2+q^2+r^2)}}, \quad (2.2)$$

and written as

$$E = \frac{1}{48} \lim_{\tau \rightarrow 0} \left(-\frac{d}{d\tau} \right) \sum_{p,q,r=-\infty}^{\infty} \left[g(p, q, r) + g(p+1/2, q+1/2, r+1/2) - 6g(p, q, q) \right. \\ \left. - 6g(p+1/2, q+1/2, q+1/2) + 8g(\sqrt{3}p/2, 0, 0) \right. \\ \left. + 3g(p, 0, 0) \right], \quad (2.3)$$

where the sums extend over all positive and negative integers including zero. (In the third and fourth terms only p and q are summed over, while in the last two terms only p is summed.) Note that the time-splitting has automatically regularized the sums, and it is easy to extract the finite part (the Epstein zeta functions Z_3 , Z_{3b} , etc. are defined in Appendix B),

$$E_L^{(D)} = \frac{1}{a} \left\{ -\frac{1}{96\pi^2} [Z_3(2; 1, 1, 1) + Z_{3b}(2; 1, 1, 1)] + \frac{1}{8\pi} \zeta(3/2) L_{-8}(3/2) + \frac{1}{16\pi} Z_{2b}(3/2; 2, 1) \right. \\ \left. - \frac{\pi}{96} - \frac{\pi\sqrt{3}}{72} \right\}, \quad (2.4)$$

where (the prime means the origin is excluded) [23]

$$\sum'_{m,n=-\infty}^{\infty} (m^2 + 2n^2)^{-s} = 2\zeta(s) L_{-8}(s). \quad (2.5)$$

The energy then evaluates numerically to

$$E_L^{(D)} = -\frac{0.0468804266}{a}. \quad (2.6)$$

The divergent parts, also extracted from the regularization procedure, follow the expected form of Weyl's law with the quartic divergence associated with the volume V , the cubic divergence associated with the surface area S , and the quadratic divergence matched with the edge coefficient

$$E_{\text{div}}^{(D)} = \frac{3V}{2\pi^2\tau^4} - \frac{S}{8\pi\tau^3} + \frac{C}{48\pi\tau^2}. \quad (2.7)$$

Here and subsequently, the edge coefficient C for a polyhedron is defined as [24]

$$C = \sum_j \left(\frac{\pi}{\alpha_j} - \frac{\alpha_j}{\pi} \right) L_j, \quad (2.8)$$

where the α_j are dihedral angles and the L_j are the corresponding edge lengths. The above expression for the divergences will be the same for all subsequent cavities with Dirichlet boundary conditions.

2. Neumann BC

In the case of Neumann boundary conditions, the complete set of mode numbers must satisfy $0 \leq k \leq m \leq n$, excluding the case when all mode numbers are zero. The Neumann Casimir energy can be defined in terms of the preceding Dirichlet result as

$$E_L^{(N)} = E_L^{(D)} - \frac{1}{8\pi a} \left[2\zeta(3/2)L_{-8}(3/2) + Z_{2b}(3/2; 2, 1) \right], \quad (2.9)$$

which gives us a numerical value of

$$E_L^{(N)} = -\frac{0.1964621484}{a}. \quad (2.10)$$

The divergent parts also match the expected Weyl terms for Neumann boundary conditions. We note that the cubic divergence's coefficient changes sign when comparing Dirichlet and Neumann divergent parts:

$$E_{\text{div}}^{(N)} = \frac{3V}{2\pi^2\tau^4} + \frac{S}{8\pi\tau^3} + \frac{C}{48\pi\tau^2}. \quad (2.11)$$

This form is also obtained for all the following calculations involving Neumann boundary conditions.

B. Medium Tetrahedron

The eigenvalue spectrum of the medium tetrahedron, shown in Fig. 2, obtained by bisecting the large tetrahedron in the $z = 0$ plane, is of the same form as that of the large tetrahedron [Eq. (2.1)] with different constraints.

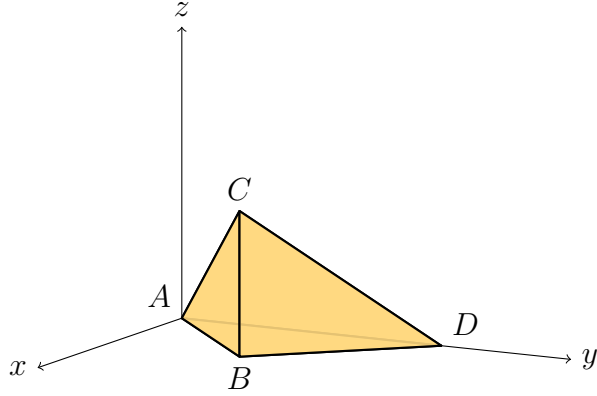


FIG. 2: Medium tetrahedron: $0 < z < x$ and $x < y < 2a - x$.

1. Dirichlet BC

The complete set of mode numbers for the Dirichlet case satisfies the constraints $0 < m < n < k < m + n$. Following the same regularization procedure used in the preceding cases, we obtain the Dirichlet Casimir energy in terms of the Dirichlet result for the large tetrahedron,

$$E_M^{(D)} = \frac{1}{2} E_L^{(D)} + \frac{1}{96\pi a} \left[3\zeta(3/2)\beta(3/2) - (1 + \sqrt{2})\pi^2 \right], \quad (2.12)$$

where we used [23]

$$\sum'_{m,n=-\infty}^{\infty} (m^2 + n^2)^{-s} = 4\zeta(s)\beta(s). \quad (2.13)$$

The Casimir energy evaluates to

$$E_M^{(D)} = -\frac{0.0799803933}{a}. \quad (2.14)$$

Here the function β is also defined in Appendix B.

2. Neumann BC

With Neumann boundary conditions, the complete set of mode numbers is restricted to $0 \leq m \leq n \leq k \leq m + n$, excluding the all-null case. As with the Dirichlet case, the Neumann Casimir energy for the medium tetrahedron can be expressed in terms of the

Neumann result for the large tetrahedron:

$$\begin{aligned}
 E_M^{(N)} &= \frac{1}{2} E_L^{(N)} - \frac{1}{96\pi a} \left[3\zeta(3/2)\beta(3/2) + (1 + \sqrt{2})\pi^2 \right] \\
 &= -\frac{0.1997008024}{a}.
 \end{aligned}
 \tag{2.15}$$

C. Small Tetrahedron

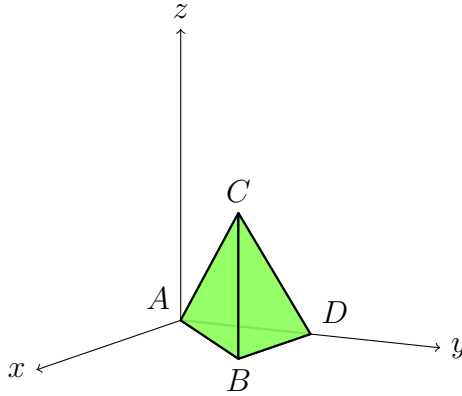


FIG. 3: Small tetrahedron: $0 < z < x$ and $x < y < a$.

The small tetrahedron (Fig. 3) may be visualized as the result of a bisection of a medium tetrahedron along the plane $y = a$. The form of the eigenvalue spectrum for the small tetrahedron is different from the previous two tetrahedra but the same as the cube's²:

$$\lambda_{kmn}^2 = \frac{\pi^2}{a^2} (k^2 + m^2 + n^2) .
 \tag{2.16}$$

The Dirichlet case is the aforementioned “pyramidal cavity” considered in Ref. [18].

² This spectrum is actually the same as that for the other tetrahedra, given in Eq. (2.1), with the additional restriction that $m + n + k$ be even.

1. Dirichlet BC

The modal restriction for the complete set is $0 < k < m < n$. The finite part obtained is thus

$$E_S^{(D)} = \frac{1}{a} \left[-\frac{1}{192\pi^2} Z_3(2; 1, 1, 1) + \frac{1}{16\pi} \zeta(3/2) L_{-8}(3/2) + \frac{1}{32\pi} \zeta(3/2) \beta(3/2) - \frac{\pi}{64} - \frac{\pi\sqrt{3}}{72} - \frac{\pi\sqrt{2}}{96} \right], \quad (2.17)$$

which evaluates to

$$E_S^{(D)} = -\frac{0.10054146218}{a}. \quad (2.18)$$

This result differs from that of Ref. [18]. The discrepancy appears to stem from a mode-counting error in Ref. [18], and the result found there is likely wrong.

2. Neumann BC

For the Neumann case, we again find the same condition that the mode numbers must satisfy $0 \leq k \leq m \leq n$ excluding the origin. The Neumann Casimir energy is derived to be

$$E_S^{(N)} = E_S^{(D)} - \frac{1}{16\pi a} \zeta(3/2) \left[2 L_{-8}(3/2) + \beta(3/2) \right], \quad (2.19)$$

with a numerical value of

$$E_S^{(N)} = -\frac{0.2587920021}{a}. \quad (2.20)$$

III. CASIMIR ENERGIES OF RECTANGULAR PARALLELEPIPEDS

Amongst the geometries considered for Casimir energy calculations, rectangular parallelepipeds are the most straightforward. Their eigenfunctions and eigenvalues are well known and as such have been subject of many articles [8–13]. We rederive a few of these results in the following paragraphs. We consider a generic rectangular parallelepiped of length a , height b , and width c . The eigenfunctions for a Dirichlet rectangular parallelepiped are the well-known products of three sine functions. The spectrum is the familiar expression

$$\lambda_{kmn}^2 = \pi^2 \left(\frac{k^2}{a^2} + \frac{m^2}{b^2} + \frac{n^2}{c^2} \right). \quad (3.1)$$

A. Dirichlet BC

The complete set of mode numbers in the Dirichlet case satisfy the restrictions $k > 0$, $m > 0$, and $n > 0$. The Casimir energy may be written in terms of Epstein zeta functions and the ratios: $\chi \equiv (b/a)^2$ and $\sigma \equiv (c/a)^2$

$$E_P^{(D)} = \frac{1}{a} \left\{ -\frac{\sqrt{\chi\sigma}}{32\pi^2} Z_3(2; 1, \chi, \sigma) + \frac{1}{64\pi} \left[\sqrt{\chi\sigma} Z_2(3/2; \chi, \sigma) + \sqrt{\sigma} Z_2(3/2; 1, \sigma) + \sqrt{\chi} Z_2(3/2; 1, \chi) \right] - \frac{\pi}{96} \left(1 + \frac{1}{\sqrt{\chi}} + \frac{1}{\sqrt{\sigma}} \right) \right\}. \quad (3.2)$$

B. Neumann BC

For Neumann boundary conditions the complete set is given by $k \geq 0$, $m \geq 0$, and $n \geq 0$, excluding the case where they are all null. In terms of the Dirichlet result we obtain

$$E_P^{(N)} = E_P^{(D)} - \frac{1}{32\pi a} \left[\sqrt{\chi\sigma} Z_2(3/2; \chi, \sigma) + \sqrt{\sigma} Z_2(3/2; 1, \sigma) + \sqrt{\chi} Z_2(3/2; 1, \chi) \right]. \quad (3.3)$$

IV. CASIMIR ENERGIES OF A CUBE

The cube is a special parallelepiped with equal length, width, and height. Our results for the generic parallelepiped therefore apply for the particular case of $a = b = c$ or $\chi = \sigma = 1$. This particular geometry has also been the subject of prior inquiries, for example Ref. [8], so we are simply rederiving these results.

A. Dirichlet BC

The Dirichlet Casimir energy for a cube of edge length a is simply

$$E_{\text{Cube}}^{(D)} = \frac{1}{a} \left[-\frac{1}{32\pi^2} Z_3(2; 1, 1, 1) + \frac{3}{16\pi} \zeta(3/2)\beta(3/2) - \frac{\pi}{32} \right], \quad (4.1)$$

from which we obtain the finite part, a result which matches that of Ref. [11]:

$$E_{\text{Cube}}^{(D)} = -\frac{0.0157321825}{a}. \quad (4.2)$$

B. Neumann BC

With the same modal restrictions as for the parallelepipedal Neumann cases, the Neumann result can be related to the Dirichlet result with

$$E_{\text{Cube}}^{(N)} = E_{\text{Cube}}^{(D)} - \frac{3}{8\pi a} \zeta(3/2) \beta(3/2), \quad (4.3)$$

which gives a numerical value already confirmed in Ref. [11]:

$$E_{\text{Cube}}^{(N)} = -\frac{0.2853094722}{a}. \quad (4.4)$$

V. CASIMIR ENERGIES OF TRIANGULAR PRISMS

Since infinite triangular prisms are soluble cases [5], one would also expect finite prisms to be soluble [20, 25]. Indeed, one can also find the interior Casimir energies of finite triangular prisms of right isosceles, equilateral, and hemiequilateral cross-sections. The spectra differ slightly from the infinite cases with the replacement of an integral over longitudinal wavenumbers by a sum over discrete longitudinal eigenvalues.

A. Right Isosceles Triangular Prism

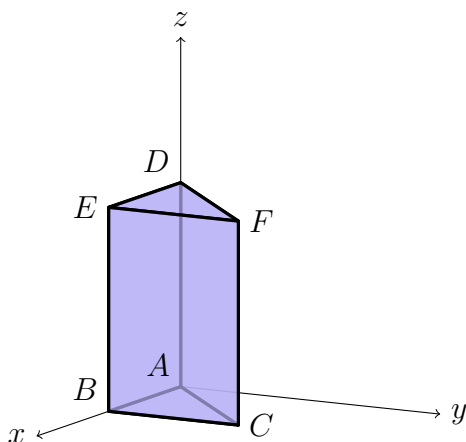


FIG. 4: Right isosceles prism. $|DE| = |EF| = a$, $|DF| = a\sqrt{2}$, and $|BE| = b$.

1. *Dirichlet BC*

The spectrum for a prism of right isosceles cross-section, illustrated in Fig. 4, is

$$\lambda_{kmn}^2 = \frac{\pi^2}{a^2}(m^2 + n^2) + \frac{\pi^2}{b^2}k^2. \quad (5.1)$$

The complete set of eigenmodes for this Dirichlet case is characterized by $0 < n < m$ and $0 < k$. The Casimir energy, in terms of $\chi \equiv (b/a)^2$, is, therefore,

$$E_{\text{RIsoP}}^{(D)} = \frac{1}{a} \left[-\frac{\sqrt{\chi}}{64\pi^2} Z_3(2; 1, 1, \chi) + \frac{1}{32\pi} \zeta(3/2)\beta(3/2) + \frac{\sqrt{\chi}}{64\pi} Z_2(3/2; 1, \chi) + \frac{\sqrt{\chi}}{32\pi} Z_2(3/2; 1, 2\chi) - \frac{\pi}{64\sqrt{\chi}} - \frac{\pi(1 + \sqrt{2})}{96} \right]. \quad (5.2)$$

2. *Neumann BC*

For the Neumann case, the constraint on the mode numbers is again less strict, with $0 \leq n \leq m$, $0 \leq k$ excluding $k = m = n = 0$. In terms of the Dirichlet result, we find:

$$E_{\text{RIsoP}}^{(N)} = E_{\text{RIsoP}}^{(D)} - \frac{1}{32\pi a} \left[2\zeta(3/2)\beta(3/2) + \sqrt{\chi} Z_2(3/2; 1, \chi) + 2\sqrt{\chi} Z_2(3/2; 1, 2\chi) \right]. \quad (5.3)$$

B. Equilateral Triangular Prism

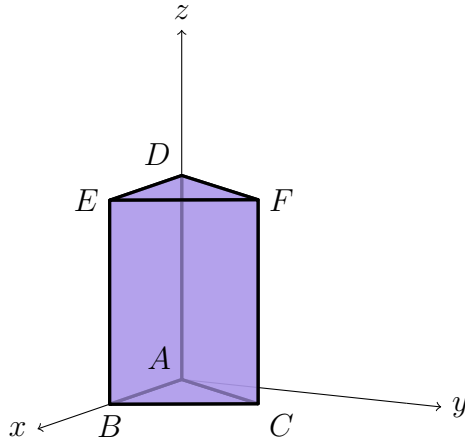


FIG. 5: Equilateral prism. $|DE| = |EF| = |FD| = a$, and $|BE| = b$.

The spectrum for an equilateral prism of height b , shown in Fig. 5, is

$$\lambda_{kmn}^2 = \frac{16\pi^2}{9a^2}(m^2 - mn + n^2) + \frac{\pi^2}{b^2}k^2. \quad (5.4)$$

1. Dirichlet BC

The constraint on k , m , and n for the complete set of modes is the same as in the Dirichlet right isosceles case. The Casimir energy, in terms of $\chi \equiv (b/a)^2$, is thus derived as

$$E_{\text{EqP}}^{(D)} = \frac{1}{a} \left\{ -\frac{\sqrt{3\chi}}{\pi^2} [Z_3(2; 3, 9, 16\chi) + Z_{3c}(2; 3, 9, 16\chi)] + \frac{5}{48\pi} \zeta(3/2) L_{-3}(3/2) + \frac{1}{24\pi} Z_{2b}(3/2; 1, 3) + \frac{3\sqrt{\chi}}{2\pi} Z_2(3/2; 9, 16\chi) - \frac{\pi}{36} - \frac{\pi}{72\sqrt{\chi}} \right\}, \quad (5.5)$$

where we used [23]

$$\sum'_{m,n=-\infty}^{\infty} (m^2 + 3n^2)^{-s} = 2(1 + 2^{1-2s})\zeta(s)L_{-3}(s). \quad (5.6)$$

This particular case was also considered earlier by Ahmedov and Duru [26], although their result appears misleading.

2. Neumann BC

The Neumann constraint is also the same as that for the Neumann right isosceles triangular prism. Similarly to previous cases, we relate the Neumann result to the Dirichlet result,

$$E_{\text{EqP}}^{(N)} = E_{\text{EqP}}^{(D)} - \frac{1}{24\pi a} \left[5\zeta(3/2)L_{-3}(3/2) + 2Z_{2b}(3/2; 1, 3) + 72\sqrt{\chi} Z_2(3/2; 9, 16\chi) \right]. \quad (5.7)$$

C. Hemiequilateral Triangular Prism

The hemiequilateral triangular prism (Fig. 6) or prism with cross-section being a triangle with angles $(\pi/2, \pi/3, \pi/6)$ shares the same spectral form as the equilateral triangular prism,

$$\lambda_{kmn}^2 = \frac{16\pi^2}{9a^2} (m^2 - mn + n^2) + \frac{\pi^2}{b^2} k^2. \quad (5.8)$$

They differ, however, in the constraints for each boundary condition.

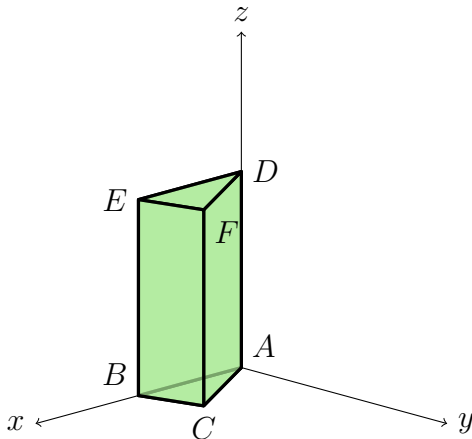


FIG. 6: Hemiequilateral prism. $|DF| = a\sqrt{3/4}$, $|EF| = a/2$, $|DE| = a$, and $|BE| = b$.

1. Dirichlet BC

The complete set of modes must satisfy $0 < k$, and $0 < n < m < 2n$. Again, in terms of $\chi \equiv (b/a)^2$, we find that the Dirichlet Casimir energy is of the form

$$E_{\text{HemP}}^{(D)} = \frac{1}{2}E_{\text{EqP}}^{(D)} + \frac{\sqrt{3\chi}}{4\pi a}Z_2(3/2; 3, 16\chi) - \frac{\pi}{72a}\left(\sqrt{3} + \frac{3}{4\sqrt{\chi}}\right). \quad (5.9)$$

2. Neumann BC

The completeness constraint for the Neumann case is again less strict than for the Dirichlet case with $0 \leq k$, $0 \leq n \leq m \leq 2n$ excluding the origin. In relation to the previous result, we write

$$E_{\text{HemP}}^{(N)} = \frac{1}{2}E_{\text{EqP}}^{(N)} - \frac{\sqrt{3\chi}}{4\pi a}Z_2(3/2; 3, 16\chi) - \frac{\pi}{72a}\left(\sqrt{3} + \frac{3}{4\sqrt{\chi}}\right). \quad (5.10)$$

VI. CASIMIR ENERGIES OF A SPHERE

The sphere is also one of the geometries most often the subject of Casimir energy calculations (For more complete references see Ref. [4].) We report results found in the literature for a sphere of radius a satisfying Dirichlet and Neumann boundary conditions. A noteworthy difference between the calculations of the energies for tetrahedra and prisms as compared to a sphere is that in the polyhedral cases only the interior modes are considered (the exterior

modes are unknown) whereas in the spherical case both interior and exterior are (necessarily) included to cancel the curvature divergences.

A. Dirichlet BC

The Dirichlet Casimir energy of a sphere is well known and may be found in Ref. [27],

$$E_{\text{Sphere}}^{(D)} = \frac{0.0028168}{a}. \quad (6.1)$$

B. Neumann BC

The Neumann result is also well known and can be found in Ref. [28],

$$E_{\text{Sphere}}^{(N)} = -\frac{0.223777}{a}. \quad (6.2)$$

VII. SYSTEMATICS OF CASIMIR ENERGIES

As indicated in the introduction, the relation between the self-energy of a system and its geometry is not obvious. (We set aside the more serious physical difficulty as to the meaning and the observability of Casimir self-energies.) Having additional data, such as the self-energies of tetrahedra and finite prisms, may help in shedding some light on this problem. Our analysis is similar to the one applied earlier to infinite prisms [5]. In terms of the volume V and the surface area S of the bodies, the dimensionless scaled Casimir energies, $E_{\text{Sc}} = E \times V/S$, are tabulated in Table I, and are plotted against the corresponding isoareal quotients, $\mathcal{Q} = 36\pi V^2/S^3$ in Fig. 7. It is also possible to look at the prisms in a more revealing light by plotting their scaled energies with respect to the parameters \mathcal{Q} and b^2/A (Fig. 8). The corresponding results for Neumann energies are given in Fig. 9.

VIII. LIMITING CASES OF PRISMS

For the prisms we considered, with square and equilateral, hemiequilateral, and right-isosceles triangular cross sections, we can examine two limits which reduce to known cases. With b as the height of the prism, the limit $b \rightarrow 0$ must coincide with the classic Casimir

Cavity	Q	$E_{Sc}^{(D)}$	$E_{Sc}^{(N)}$
Small T.	0.22327	-0.00694	-0.01787
Medium T.	0.22395	-0.00696	-0.01739
Large T.	0.27768	-0.00552	-0.02315
Cube	0.52359	-0.00262	-0.04755
Spherical Shell	1	0.00093	-0.07459

TABLE I: Scaled energies and isoareal quotients.

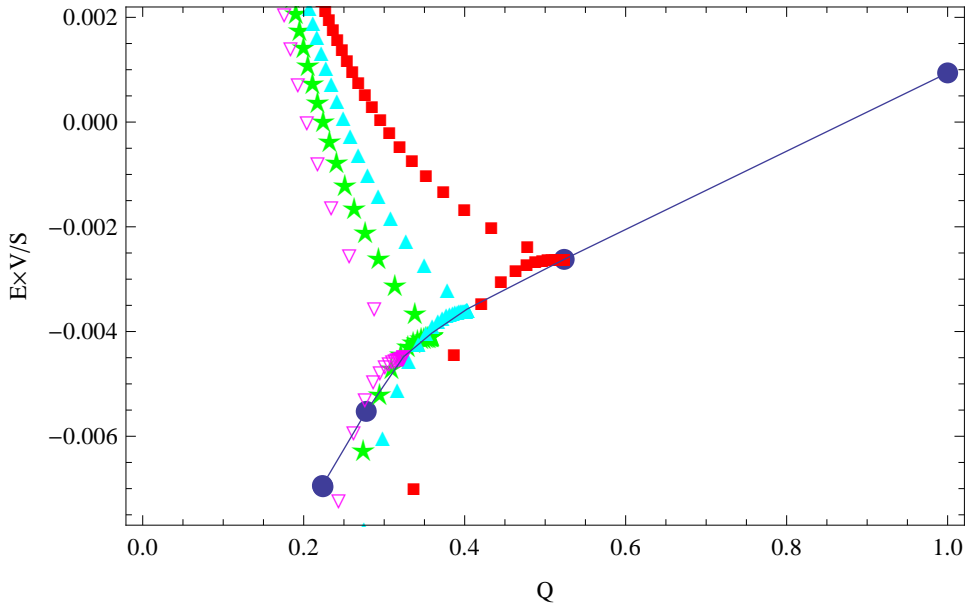


FIG. 7: Scaled Dirichlet energies vs. isoareal quotients. From left to right, the circular markers indicate results for the small and medium tetrahedra (which cannot be resolved on this graph), the large tetrahedron, the cube, and the sphere. The square, filled triangle, star, and empty triangle markers correspond respectively to square prisms (parallelepipeds with $\sigma = 1$), and equilateral, right isosceles, and hemiequilateral triangular prisms, respectively. The prism energies become more negative for $b \rightarrow 0$, less negative for $b \rightarrow \infty$. Note that the cusps, corresponding to the maximal isoareal coefficient for a given class of cylinders, also lie close to a universal curve that passes through the tetrahedral points.

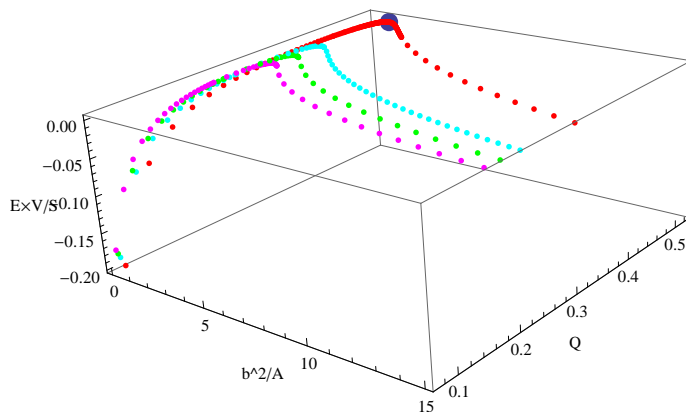


FIG. 8: Scaled Dirichlet energies of prisms vs. isoareal quotients Q and b^2/A , where A is the cross-sectional area. Starting from the lowest Q -values, the curves correspond respectively to hemiequilateral, right isosceles, and equilateral triangular prisms, and square prisms (parallelepipeds with $\sigma = 1$). The square prisms' curve goes through the cube's data point (displayed prominently).

case of parallel plates of area A ,

$$E \rightarrow -\frac{\pi^2}{1440b^3}A. \quad (8.1)$$

And with $b \rightarrow \infty$ we must recover the energy for infinite cylinders given in Ref. [5],

$$E \rightarrow \mathcal{E}_{\text{cyl}}b, \quad (8.2)$$

in terms of the energy/length for the cylinder, \mathcal{E}_{cyl} . For a prism of cross section A and cross-sectional perimeter P , the scaled Casimir energy is

$$E_{\text{Sc}} = E \frac{V}{S} = \frac{EA b}{(2A + Pb)}, \quad (8.3)$$

where S denotes the total surface area of the prism and V its volume. Thus, in the limit of vanishing height,

$$b \rightarrow 0 : \quad E_{\text{Sc}} \rightarrow -\frac{\pi^2}{2880} \frac{A}{b^2}. \quad (8.4)$$

In the limit of infinite length,

$$b \rightarrow \infty : \quad E_{\text{Sc}} \rightarrow (\mathcal{E}_{\text{cyl}}b) \frac{A}{P}. \quad (8.5)$$

These limits are exact.

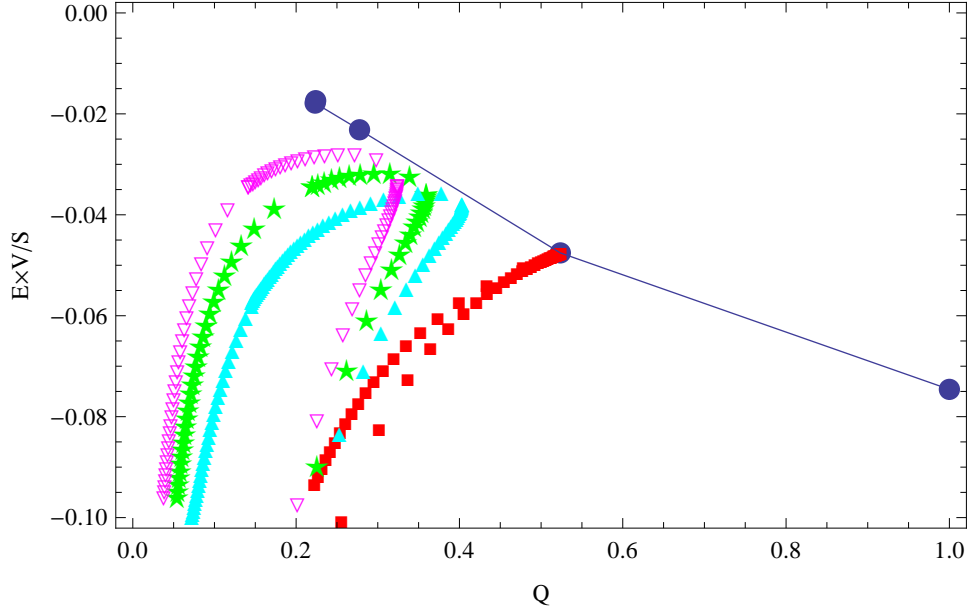


FIG. 9: Scaled Neumann energies vs. isoareal quotients. From left to right, the circular markers indicate results for the small and medium tetrahedra (which cannot be resolved on this graph), the large tetrahedron, the cube, and the sphere. The square, filled triangle, star, and empty triangle markers correspond respectively to square prisms (parallelepipeds with $\sigma = 1$), and equilateral, right isosceles, and hemiequilateral triangular prisms, respectively. The energies in this case are always negative. Note that the cusps, corresponding to the maximal isoareal coefficient for a given class of cylinders, again lie close to a universal curve that passes through the tetrahedral points.

It may be interesting to express these limits in terms of the isoareal quotients:

$$Q = \frac{36\pi V^2}{S^3} = \frac{36\pi b^2 A^2}{(2A + bP)^3}, \quad (8.6)$$

whence,

$$b \rightarrow 0: \quad E_{\text{Sc}} \rightarrow -\frac{\pi^3}{640Q}. \quad (8.7)$$

In this limit $Q \rightarrow 0$. A similar expression may be obtained in the large b limit if we use the proximity force approximation as discussed in Ref. [5]:

$$\mathcal{E}_{\text{cyl}} A \approx \frac{\pi^2}{368640} \left(\frac{P^2}{A} \right)^2, \quad (8.8)$$

which becomes exact as the smallest angle of the triangle vanishes. In this approximation

$$b \rightarrow \infty : \quad E_{\text{Sc}} \approx \frac{\pi^3}{10240} \frac{1}{\mathcal{Q}}, \quad (8.9)$$

where again $\mathcal{Q} \rightarrow 0$. In Fig. 10 we show how the long and short prism limit are approached by our data.

Let us examine the $b \rightarrow 0$ limit for the example of the square prism, where the Dirichlet energy is given by Eq. (3.2), with $\sigma = 1$. Using the Euler-Maclaurin summation formula, we find the asymptotic limit of that expression for short prisms to be

$$E_{\text{Sq}}^D \sim -\frac{\pi^2 a^2}{1440 b^3} \left[1 - \frac{90 b}{\pi^3 a} \zeta(3) + \frac{15 b^2}{\pi a^2} \right], \quad b/a \rightarrow 0. \quad (8.10)$$

There are only exponentially small corrections to this result. Similarly in the long distance (infinitely long cylinder) limit, $b \gg a = c$,

$$E_{\text{Sq}}^D \sim -\frac{1}{16\pi a} \left\{ \frac{b}{a} \left[\frac{\pi}{3} G - \zeta(3) \right] - \left[\zeta(3/2) \beta(3/2) - \frac{\pi^2}{3} \right] \right\}, \quad a/b \rightarrow 0, \quad (8.11)$$

again, up to exponentially small terms. (Here G is Catalan's constant.) Note that the leading terms in the expressions are the correct limiting forms: that in Eq. (8.10) is Casimir's result for plates of area a^2 , and that in Eq. (8.11) is that for a square cylinder found in Eq. (5.4) of Ref. [5]. In Fig. 11 we plot, parametrically, these asymptotic limits against the exact form of the isoareal coefficient, e.g. $\mathcal{Q} = 9\pi b^2 a / 2(a + 2b)^3$ for the square prism. We note that both limiting forms are well reproduced by the data for the prisms, all the way down to the cusp which occurs for the maximal value of the isoareal coefficient. In fact, the accuracy of the asymptotic formulas is remarkable: At the cusp, $b = a$, Eq. (8.10) gives for the scaled energy of the cube the value -0.00261078 , while Eq. (8.11) gives -0.00261479 , both differing by less than 0.5% from the exact value -0.00262203 .

IX. CONCLUSIONS

In this paper, we have extended the work of Ref. [5] from infinite cylinders to finite prisms and to integrable tetrahedra. The previous work was essentially two dimensional, so it was possible to give closed form results for the Casimir self energy. This is apparently not possible, at least not currently, for the cases considered in this paper. Nevertheless, our answers are expressed in terms of Epstein zeta functions and other well-known functions, so numerical results of arbitrary accuracy are available.

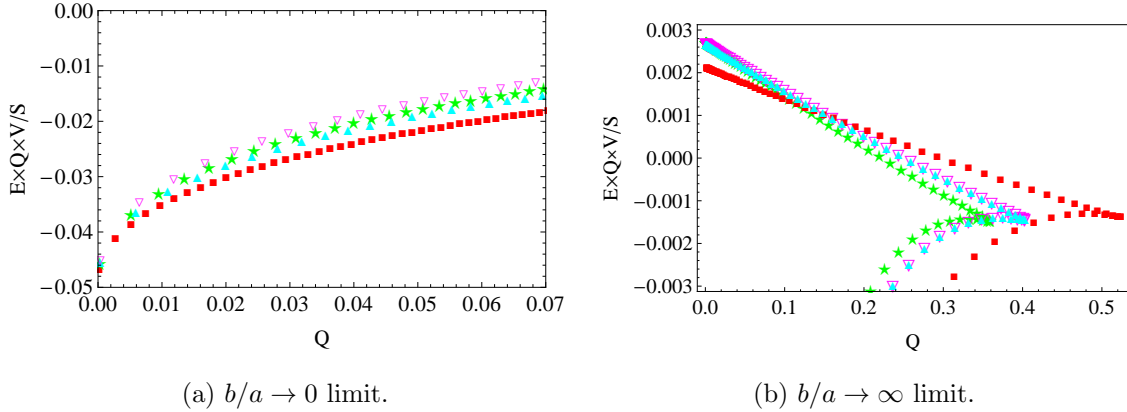


FIG. 10: EQV/S plotted versus Q in the $b/a \rightarrow 0$ (left panel) and $b/a \rightarrow \infty$ (right panel) limits for Dirichlet prisms. The curves consisting of square, filled triangle, star, and empty triangle markers correspond respectively to prisms of square, and equilateral, right isosceles, and hemiequilateral triangular cross-sections. The curves converge to the expected value of $-\pi^3/640 = -0.0484473$ as $b/a \rightarrow 0$. In the $b/a \rightarrow \infty$ limit, they converge respectively to the values of 0.00213, 0.00269, 0.00274, and 0.00277 which are simply obtained from Eq. (8.5). These limits are not particularly close to the proximity force approximation value of $\pi^3/10240 = 0.00303$.

The emerging systematics are very intriguing: Not only do the three integrable tetrahedra and the cube and the sphere seem to lie very close to a universal curve (there is a very slight discrepancy in the case of the small/medium tetrahedra) but the maximal isoareal limits of the triangular prisms line up as well. The square prisms are well described by the asymptotic formulæ (8.10) and (8.11), and similar formulæ exist for the other prisms. These results are not yet conclusive, since the cases we can evaluate are limited. Numerical work will have to be done to explore the geometrical dependence of the Casimir energy of cavities composed of flat surfaces of arbitrary shape.

The reader may rightly inquire as to what the physical significance of these results may be. Self-energies are inherently resistant to physical observation: they describe the energy required to assemble the configuration, but not the energy required to remove one side of a box, for example. And, here, the difficulty of interpretation is somewhat compounded, since we are unable to include effects of the modes exterior to the cavity. For the case of a sphere or a cylinder, it is inconsistent not to do so, since a unique finite result cannot be obtained except for a shell of infinitesimal thickness, with both interior and exterior

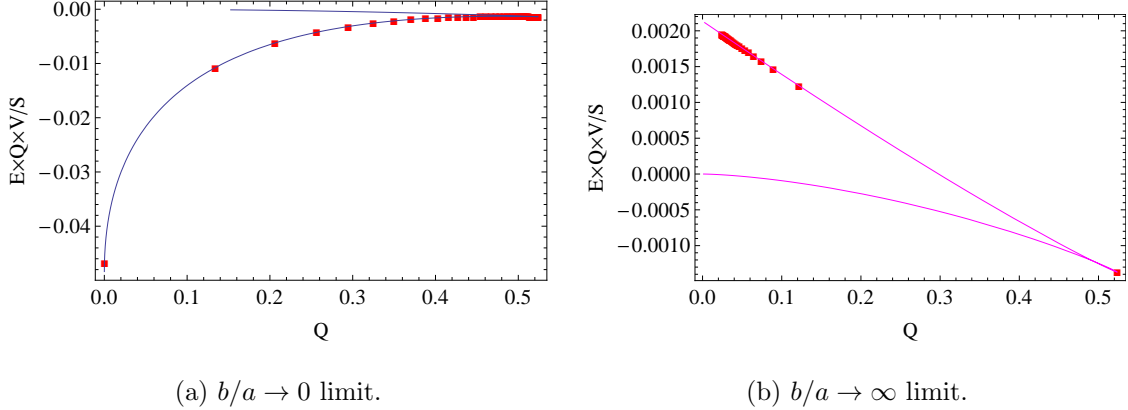


FIG. 11: Asymptotic fits for square prisms. The small height ($b/a \rightarrow 0$) (left panel) and large height ($b/a \rightarrow \infty$) (right panel) asymptotic energies are shown, corresponding to Eqs. (8.10) and (8.11), respectively. Plotted is the energy multiplied by QV/S , as a function of Q . The square markers show the exact results, which lie very close to the physical branch in each case.

contributions. Here, however, we are considering cavities with flat sides, so an unambiguous finite part may be extracted, with the volume, surface, and corner Weyl divergences uniquely removable. Curvature divergences correspond to a logarithmic divergence in the energy, so they introduce an arbitrary scale, and there is no meaning to interior and exterior mode contributions separately.

The fact that these interior energies are rigorously computable and exude a sense of overall order is already an important step. One could very well rephrase this problem in terms of cavities in conducting materials, where the exterior would not be of significance. In fact, we argue that one would only need to compute the interior energies of arbitrary domains with planar boundaries to observe significant patterns. Even then, the converse problem for domains with smooth boundaries in conducting materials would still arise. It is very likely the solution lies in the transition from planar to smooth boundaries, from discreteness to continuity. Nevertheless, it is remarkable, even though it appears fortuitous, that our results for tetrahedra and prisms appear to lie on a curve which intercepts the interior plus exterior Casimir energy for a sphere. The answers are most surely rooted in what happens in between, and the appearance of the curvature-related logarithmic terms. The zero-point energies for spheres are considered purely in the spirit of future analyses.

At the very least, the work reported here is of mathematical interest in elucidating the systematics of Casimir energies. In Ref. [27], we explored the systematic dependence on di-

mension for hyperspheres. Here, we have discovered some remarkable systematic behavior, where the values of Casimir energies vary smoothly with geometrical parameters. Understanding such systematics is vital for future developments involving quantum vacuum effects, which will undoubtedly yield applications in nanoscience [29].

In addition to the worthwhile issues raised in the previous paragraphs, work on other boundary conditions, in particular electromagnetic boundary conditions, is currently under way. Unlike for cylinders, the electromagnetic energy of a tetrahedron is not merely the sum of Dirichlet and Neumann parts; there is no break-up into TE and TM modes in general. So this is a formidable task. Higher-dimensional analogues, polytopes, are also currently the subject of ongoing work.

Acknowledgments

We thank the US National Science Foundation and the US Department of Energy for partial support of this work. We further thank Nima Pourtolami and Prachi Parashar for collaborative assistance.

Appendix A: Poisson Resummation Formulae

We consider the Poisson resummation of the traced cylinder kernel of an arbitrary real quadratic form,

$$\mathcal{S} = \sum_{m_1, \dots, m_n = -\infty}^{\infty} e^{-\tau \sqrt{(m+a)_j A_{jk} (m+a)_k}}. \quad (\text{A1})$$

Taking the Fourier transform of the summand of \mathcal{S} and using Eq. (1.2) gives

$$\mathcal{S} = \sum_{m_1, \dots, m_n = -\infty}^{\infty} \int_{-\infty}^{\infty} \prod_{j=1}^n du_j e^{2\pi i u_j m_j} e^{-\tau \sqrt{(u_i + a_i) A_{ik} (u_k + a_k)}}. \quad (\text{A2})$$

We shift the variables

$$u_j \rightarrow u_j - a_j, \quad (\text{A3})$$

and diagonalize A

$$B_{ij} = U_{ik} A_{km} U_{mj}^T. \quad (\text{A4})$$

A redefinition of the integration variables follows,

$$v_j = U_{jk} u_k, \quad (\text{A5})$$

as well as the summation variables,

$$q_j = U_{jk} m_k . \quad (\text{A6})$$

As a result of these transformations, we recognize that the Jacobian of the transformation matrix is unity,

$$\prod_{j=1}^n du_j = \prod_{j=1}^n dv_j . \quad (\text{A7})$$

We are now ready to change to hyperspherical coordinates. First, we define

$$R_j = \sqrt{B_{jj}} v_j \quad (\text{A8})$$

and

$$k_j = \frac{q_j}{\sqrt{B_{jj}}} \quad (\text{A9})$$

which allows us to write

$$v_j q_j = kR \cos \theta . \quad (\text{A10})$$

Effectuating the change of variables gives us

$$\prod_{j=1}^n dv_j = |\det(B)|^{-1/2} R^{n-1} dR d\phi (\sin \theta)^{n-2} d\theta \prod_{j=1}^{n-3} (\sin \theta_j)^j d\theta_j . \quad (\text{A11})$$

The ϕ -integral produces a 2π and the integrals for the first $(n-3)$ θ_j angles give

$$\prod_{j=1}^{n-3} \left(\int_0^\pi \sin^j \theta d\theta \right) = \frac{\pi^{(n-3)/2}}{\Gamma((n-1)/2)} . \quad (\text{A12})$$

We are now able to focus on the remaining θ -integral,

$$\int_0^\pi (\sin \theta)^{n-2} e^{2\pi i k R \cos \theta} d\theta = \pi^{(3-n)/2} \Gamma((n-1)/2) (kR)^{(2-n)/2} J_{(n-2)/2}(2\pi kR) . \quad (\text{A13})$$

The last integral, the R -integral, is evaluated rather straightforwardly,

$$\int_0^\infty dR R^{n/2} J_{(n-2)/2}(2\pi kR) e^{-\tau R} = \frac{\tau^{2^{n-1}} \pi^{(n-3)/2} k^{(n-2)/2} \Gamma((n-1)/2)}{(\tau^2 + 4\pi^2 k_j k_j)^{(n+1)/2}} , \quad (\text{A14})$$

and putting everything together we obtain:

$$\mathcal{S} = \frac{2^n \pi^{(n-1)/2} \Gamma((n+1)/2)}{|\det(A)|^{1/2}} \sum_{m_1, \dots, m_n = -\infty}^{\infty} \frac{\tau e^{-2\pi i m_j a_j}}{(\tau^2 + 4\pi^2 k_j k_j)^{(n+1)/2}} . \quad (\text{A15})$$

From this result we obtain the following resummed expressions we use in the paper:

$$\left(-\frac{d}{d\tau}\right) \sum_{p,q,r=-\infty}^{\infty} e^{-\tau\sqrt{\alpha(p+a)^2+\beta(q+b)^2+\gamma(r+c)^2}} = \frac{24\pi}{\sqrt{\alpha\beta\gamma}\tau^4} - \frac{1}{2\pi^3\sqrt{\alpha\beta\gamma}} \quad (\text{A16})$$

$$\times \sum'_{p,q,r=-\infty}^{\infty} \left(\frac{e^{-2\pi i(pa+qb+rc)}}{(p^2/\alpha + q^2/\beta + r^2/\gamma)^2} \right),$$

$$\left(-\frac{d}{d\tau}\right) \sum_{p,q=-\infty}^{\infty} e^{-\tau\sqrt{\alpha(p+a)^2+\beta(q+b)^2}} = \frac{4\pi}{\sqrt{\alpha\beta}\tau^3} - \frac{1}{4\pi^2\sqrt{\alpha\beta}} \sum'_{p,q=-\infty}^{\infty} \frac{e^{-2\pi i(pa+qb)}}{(p^2/\alpha + q^2/\beta)^{3/2}}, \quad (\text{A17})$$

$$\left(-\frac{d}{d\tau}\right) \sum_{p=-\infty}^{\infty} e^{-\tau\sqrt{\alpha(p+a)^2}} = \frac{2}{\sqrt{\alpha}\tau^2} - \frac{\sqrt{\alpha}}{2\pi^2} \sum'_{p=-\infty}^{\infty} \frac{e^{-2\pi i(pa)}}{p^2}. \quad (\text{A18})$$

Here the prime means that all positive and negative integers are included in the sum, but not the case where all the integers are zero.

Appendix B: Epstein Zeta Functions

We define the following Epstein zeta functions:

$$Z_3(s; a, b, c) = \sum'_{k,m,n=-\infty}^{\infty} (ak^2 + bm^2 + cn^2)^{-s}, \quad (\text{B1})$$

$$Z_{3b}(s; a, b, c) = \sum'_{k,m,n=-\infty}^{\infty} (-1)^{k+m+n} (ak^2 + bm^2 + cn^2)^{-s}, \quad (\text{B2})$$

$$Z_{3c}(s; a, b, c) = \sum'_{k,m,n=-\infty}^{\infty} (-1)^{k+m} (ak^2 + bm^2 + cn^2)^{-s}, \quad (\text{B3})$$

$$Z_{2b}(s; a, b) = \sum'_{m,n=-\infty}^{\infty} (-1)^{m+n} (am^2 + bn^2)^{-s}. \quad (\text{B4})$$

Here, sums are over all integers, positive, negative, and zero, excluding the single point where all are zero. They are summed numerically using Ewald's method [23, 30, 31]. A few specific values needed for calculations:

$$Z_3(2; 1, 1, 1) = 16.5323159598, \quad (\text{B5})$$

$$Z_{3b}(2; 1, 1, 1) = -3.8631638072, \quad (\text{B6})$$

$$Z_{3c}(2; 1, 1, 1) = -1.8973804658, \quad (\text{B7})$$

$$Z_{2b}(3/2; 1, 2) = -1.9367356117, \quad (\text{B8})$$

$$Z_{2b}(3/2; 1, 3) = -1.8390292892. \quad (\text{B9})$$

The Dirichlet L -series are defined as $L_k(s) = \sum_{n=1}^{\infty} \chi_k(n) n^{-s}$ where χ_k is the number-theoretic character [23]. The Dirichlet beta function, also known as L_{-4} , is usually defined as $\beta(s) = \sum_{n=0}^{\infty} (-1)^n (2n+1)^{-s}$.

- [1] H. B. G. Casimir, Proc. Kon. Ned. Akad. Wetensch. **51**, 793 (1948).
- [2] H. B. G. Casimir, Physica **19**, 846 (1953).
- [3] T. H. Boyer, Phys. Rev. **174**, 1764 (1968).
- [4] K. A. Milton, in Lecture Notes in Physics, vol. 834: *Casimir Physics*, eds. Diego Dalvit, Peter Milonni, David Roberts, and Felipe da Rosa (Springer, Berlin, 2011), pp. 39–91 [arXiv:1005.0031].
- [5] E. K. Abalo, K. A. Milton, and L. Kaplan, Phys. Rev. D **82**, 125007 (2010).
- [6] K. A. Milton and J. Schwinger, *Electromagnetic Radiation: Variational Methods, Waveguides and Accelerators* (Springer, 2006).
- [7] J. Schwinger, L. L. DeRaad, Jr., K. A. Milton, and W.-y. Tsai, *Classical Electrodynamics* (Westview Press, 1998).
- [8] W. Lukosz, Physica **56**, 109 (1971).
- [9] W. Lukosz, Z. Phys. **258**, 99 (1973).
- [10] W. Lukosz, Z. Phys. **262**, 327 (1973).
- [11] J. Ambjørn and S. Wolfram, Ann. Phys. (NY) **147**, 1 (1983).
- [12] J. R. Ruggiero, A. H. Zimmerman, and A. Villani, Rev. Bras. Fiz. **7**, 663 (1977).
- [13] J. R. Ruggiero, A. H. Zimmerman, and A. Villani, J. Phys. A **13**, 361 (1980).
- [14] S. A. Fulling, K. A. Milton, P. Parashar, A. Romeo, K. V. Shajesh and J. Wagner, Phys. Rev. D **76**, 025004 (2007) [hep-th/0702091 [HEP-TH]].
- [15] K. V. Shajesh, K. A. Milton, P. Parashar and J. A. Wagner, J. Phys. A **41**, 164058 (2008) [arXiv:0711.1206 [hep-th]].
- [16] K. A. Milton, P. Parashar, K. V. Shajesh and J. Wagner, J. Phys. A **40**, 10935 (2007) [arXiv:0705.2611 [hep-th]].

- [17] K. A. Milton, *Phys. Rev. D* **22**, 1441 (1980).
- [18] H. Ahmedov and I. H. Duru, *J. Math. Phys.* **46**, 022303 (2005).
- [19] S. A. Fulling, *J. Phys. A* **36**, 6857 (2003).
- [20] R. Terras and R. Swanson, *J. Math. Phys.* **21**, 2140 (1980).
- [21] J. W. Turner, *J. Phys. A: Math. Gen.* **17**, 2791 (1984).
- [22] H. R. Krishnamurthy et al., *J. Phys. A: Math. Gen.* **15**, 2131 (1982).
- [23] M. L. Glasser and I. J. Zucker, *Theoretical Chemistry: Advances and Perspectives* (Academic, New York, 1980), Vol. 5, p. 67.
- [24] B. V. Fedosov, *Sov. Math. Dokl.* **4**, 1092 (1963).
- [25] R. Terras, *Math. Proc. Camb. Phil. Soc.* **89**, 331 (1981).
- [26] H. Ahmedov and I. H. Duru, *Turk. J. Phys.* **30**, 345 (2006).
- [27] C. M. Bender and K. A. Milton, *Phys. Rev. D* **50**, 6547 (1994).
- [28] V. V. Nesterenko and I. G. Pirozhenko, *Phys. Rev. D* **57**, 1284 (1998).
- [29] C. Binns, *Introduction to Nanoscience and Nanotechnology* (Wiley, Hoboken, 2010).
- [30] R. E. Crandall, *Exp. Math.* **8**, 367 (1999).
- [31] R. E. Crandall, <http://people.reed.edu/~crandall/papers/epstein.pdf> (1998).